ENHANCED GRAVITROPISM 2 encodes a STERILE ALPHA MOTIF–containing protein that controls root growth angle in barley and wheat

Gwendolyn K. Kirschner[a,1], Serena Rosignoli[b,1], Li Guo[a,1], Isaia Vardanega[a,b], Jafargholi Imani[c], Janine Altmüller[d], Sara G. Milner[e], Raffaella Balzano[b], Kerstin A. Nagel[f], Daniel Pflugfelder[f], Cristian Forestan[b], Riccardo Bovina[b], Robert Koller[f], Tyll G. Stöcker[g], Martin Mascher[e,h], James Simmonds[i], Cristobal Uauy[i], Heiko Schoof[g], Roberto Tuberosa[b], Silvio Salvi[b,2], and Frank Hochholdinger[a,2]

[a]Institute of Crop Sciences and Resource Conservation, Crop Functional Genomics, University of Bonn, 53113 Bonn, Germany; [b]Department of Agricultural and Food Sciences, University of Bologna, 40127 Bologna, Italy; [c]Institute of Phytopathology, Research Centre for BioSystems, Land Use and Nutrition, Justus-Liebig-University Giessen, 35392 Giessen, Germany; [d]Cologne Center for Genomics, University of Cologne, 50931 Cologne, Germany; [e]Leibniz Institute of Plant Genetics and Crop Plant Research Gatersleben, 06466 Seeland, Germany; [f]Institute of Bio- and Geosciences, IBG-2: Plant Sciences, Forschungszentrum Juelich GmbH, 52425 Jülich, Germany; [g]Institute of Crop Sciences and Resource Conservation, Crop Bioinformatics, University of Bonn, 53115 Bonn, Germany; [h]German Centre for Integrative Biodiversity Research Halle-Jena-Leipzig, 04103 Leipzig, Germany; and [i]John Innes Centre, Norwich Research Park, Norwich NR4 7UH, United Kingdom

Edited by Philip N. Benfey, Duke University, Durham, NC, and approved July 13, 2021 (received for review January 25, 2021)

The root growth angle defines how roots grow toward the gravity vector and is among the most important determinants of root system architecture. It controls water uptake capacity, nutrient use efficiency, stress resilience, and, as a consequence, yield of crop plants. We demonstrated that the *egt2* (*enhanced gravitropism 2*) mutant of barley exhibits steeper root growth of seminal and lateral roots and an auxin-independent higher responsiveness to gravity compared to wild-type plants. We cloned the *EGT2* gene by a combination of bulked-segregant analysis and whole genome sequencing. Subsequent validation experiments by an independent CRISPR/Cas9 mutant allele demonstrated that *egt2* encodes a STERILE ALPHA MOTIF domain–containing protein. In situ hybridization experiments illustrated that *EGT2* is expressed from the root cap to the elongation zone. We demonstrated the evolutionary conserved role of *EGT2* in root growth angle control between barley and wheat by knocking out the *EGT2* orthologs in the A and B genomes of tetraploid durum wheat. By combining laser capture microdissection with RNA sequencing, we observed that seven expansin genes were transcriptionally down-regulated in the elongation zone. This is consistent with a role of *EGT2* in this region of the root where the effect of gravity sensing is executed by differential cell elongation. Our findings suggest that *EGT2* is an evolutionary conserved regulator of root growth angle in barley and wheat that could be a valuable target for root-based crop improvement strategies in cereals.

barley | CRISPR/Cas9 | EGT2 | gravitropism | root angle

The increase in human population and climate change are major challenges to food security (1, 2). A number of studies proposed to modify root system architecture to improve water and nutrient use efficiency, crop yield, and resilience to stress episodes (3, 4). Among the most important determinants of root system architecture is the root growth angle, i.e., the angle in which roots grow toward the ground.

Increased response to gravity, or hypergravitropism, and thereby a steeper root growth angle was shown to be associated to improved drought resistance in rice, probably by increased access to deep-soil water (5). At the same time, a deeper root system facilitates the uptake of N and other mobile nutrients that are more abundant in deeper soil layers (6). Root gravitropism is regulated by sensing the gravitropic stimulus and subsequent differential cell elongation to enable root growth toward the gravitropic vector. Removing the root cap mechanically or genetically substantially diminishes the gravitropic response (7–9), suggesting that gravity sensing occurs primarily in the root cap. However, there is evidence for a sensing site outside the root cap, located in the elongation zone (10, 11). There are different hypotheses on how the cells sense gravity, with the prevailing idea that the starch-containing plastids in the root cap act as statoliths and settle in response to gravity. In doing so, they trigger a signaling cascade, either by mechanosensitive channels or by direct protein interaction, on the organelle surface (12–14). This signaling pathway ultimately leads to a rearrangement of auxin export carriers and thereby to a reorganization of the auxin maximum in the root tip (15). At the same time, changes of pH in the root cap and an asymmetrical change of pH in the upper and lower side of the root meristem and elongation zone occur (16, 17). This finally leads to an increased elongation of the cells on the side averted to the gravity vector in the elongation zone of the roots so that the roots grow downward (18). To date, only single components of the signaling cascade regulating root gravitropism have been unraveled. Examples include the actin-binding protein RICE MORPHOLOGY DETERMINANT that localizes to the surface of statoliths in rice root cap cells and controls the root growth angle in response to external phosphate (19). Another protein involved in gravitropism is the membrane-localized ALTERED RESPONSE TO GRAVITY1 in *Arabidopsis*, which is expressed in the root cap and is involved in

Significance

To date, the potential of utilizing root traits in plant breeding remains largely untapped. In this study, we cloned and characterized the *ENHANCED GRAVITROPISM2* (*EGT2*) gene of barley that encodes a STERILE ALPHA MOTIF domain–containing protein. We demonstrated that *EGT2* is a key gene of root growth angle regulation in response to gravity, which is conserved in barley and wheat and could be a promising target for crop improvement in cereals.

Author contributions: G.K.K., S.R., S.S., and F.H. designed research; G.K.K., S.R., L.G., I.V., J.I., J.A., S.G.M., R. Balzano, D.P., C.F., R. Bovina, and J.S. performed research; G.K.K., K.A.N., R.K., T.G.S., M.M., C.U., H.S., R.T., S.S., and F.H. analyzed data; and G.K.K., S.R., S.S., and F.H. wrote the paper.

The authors declare no competing interest.

This article is a PNAS Direct Submission.

[1]G.K.K., S.R., and L.G. contributed equally to this work.

[2]To whom correspondence may be addressed. Email: hochhold@uni-bonn.de or silvio.salvi@unibo.it.

This article contains supporting information online at https://www.pnas.org/lookup/suppl/doi:10.1073/pnas.2101526118/-/DCSupplemental.

Published August 26, 2021.

the gravity-induced lateral auxin gradient (20). Both proteins seem to function in signaling immediately after gravity sensing in the root cap. In contrast, rice *DEEPER ROOTING1* (*DRO1*) acts as early auxin response gene later in the gravitropic signaling. The *DRO1* gene encodes for a plasma membrane protein that is expressed in the root meristem and was identified because of its influence on the root growth angle (5). The role of DRO1 may not be conserved in primary roots of different plant species since the *Arabidopsis* homolog does not affect the gravitropic response of the primary root but influences the growth angle of the lateral roots (21).

Barley (*Hordeum vulgare*) is the world's fourth most important cereal crop in terms of grain production, after wheat (*Triticum aestivum*), rice (*Oryza sativa*), and maize (*Zea mays*) (2019, http://www.fao.org/faostat/en/). It is cultivated over a broad geographical area because it can adapt to a wide range of climatic conditions and is therefore an excellent model to study responses to

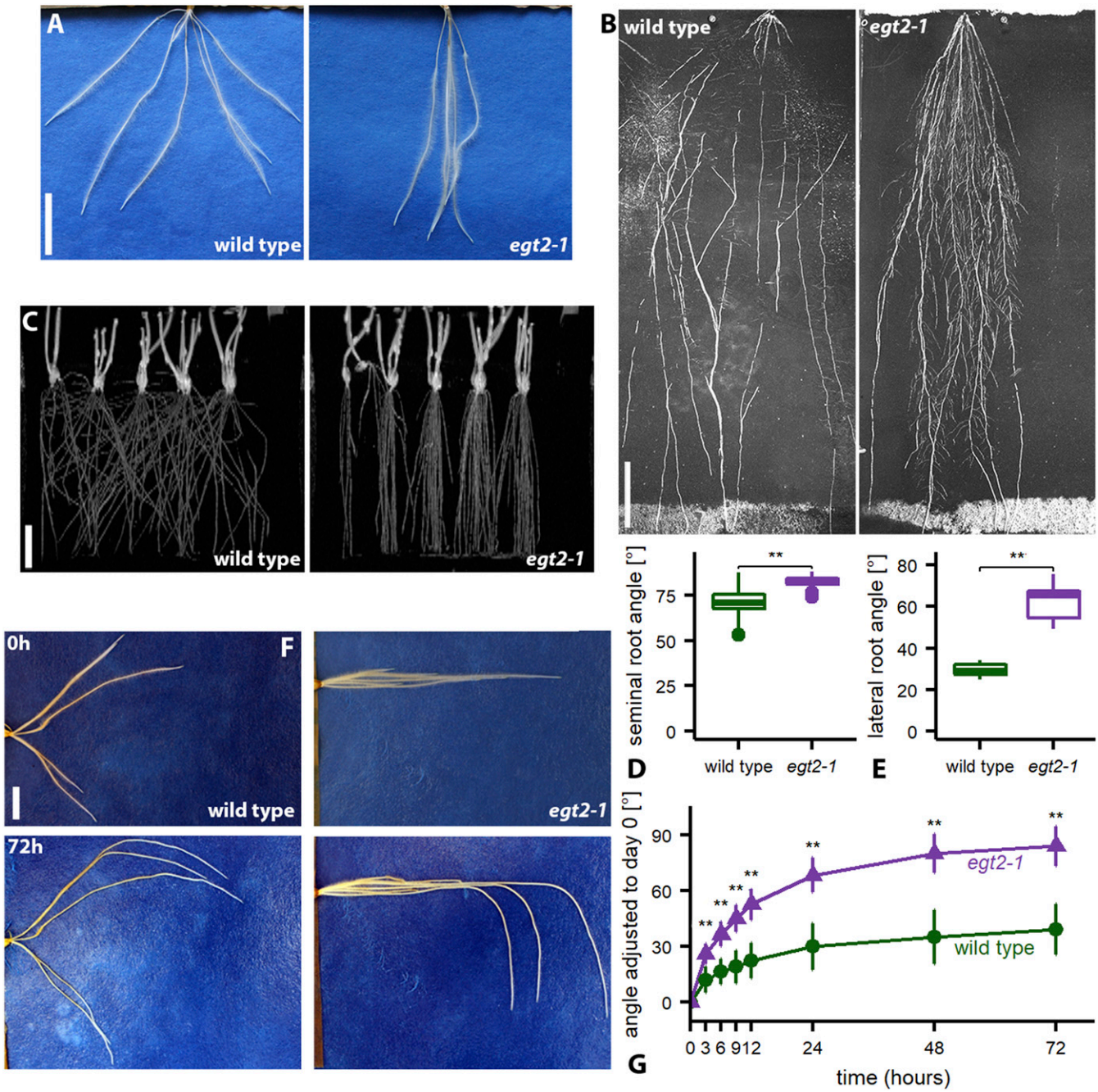

Fig. 1. Root phenotype of *egt2-1*. (*A*) Wild-type and *egt2-1* roots grown on germination paper, 7 d after germination (DAG). (Scale bar: 2 cm.) (*B*) Wild-type and *egt2-1* roots grown in rhizotrons 26 DAG. (Scale bar: 10 cm.) (*C*) MRI pictures of wild-type and *egt2-1* plants grown in soil 3 DAG. (Scale bar: 4 cm.) (*D*) Root angle of seminal roots 7 DAG; $n = 40$ per genotype in one experiment; two-tailed *t* test, $^{**}P < 0.01$. (*E*) Lateral root angle 14 DAG; n = 8 to 9 per genotype in two independent experiments; two-tailed *t* test, $^{**}P < 0.01$. (*F*) Wild-type and *egt2-1* roots after rotation (time point 0) at indicated time points. (Scale bar: 1 cm.) (*G*) Root tip angle after rotation; plants 5 DAG were rotated by 90° (time 0), and the root tip angle was measured over time; $n = 38$ per genotype in three independent experiments; the two genotypes were compared between each other at the respective time points by a two-tailed *t* test, $^{**}P < 0.01$. SD is depicted; to account for the different starting angles of the roots, all measurements were normalized to the starting angle of the roots at time 0.

climate change (22). In this study, we used a forward-genetics approach to clone *ENHANCED GRAVITROPISM2* (*EGT2*), a gene involved in barley root gravitropic response and whose effect is conserved in wheat. *EGT2* encodes a STERILE ALPHA MOTIF (SAM) domain–containing protein and likely acts in a regulatory pathway that counteracts the auxin-mediated positive gravitropic signaling pathway.

Results

The *egt2-1* Mutant Shows a Steeper Root Growth Correlated with an Enhanced Gravitropic Response. The *egt2-1* mutant was discovered in a sodium-azide mutagenized population of the barley cultivar Morex based on the hypergravitropic growth of its seminal root system in paper rolls and was shown to be inherited as a monogenic recessive Mendelian locus (23, 24). We investigated the phenotype in more detail in 2-D rhizoboxes, in which the plants grow vertically on flat filter paper. While in Morex wild type the seminal roots grow in a shallow angle toward the gravity vector and cover a larger area, the seminal roots in the *egt2-1* mutant grow steeply down (Fig. 1 *A* and *D* and *SI Appendix*, Fig. S1*A*). This phenotype was consistent in plants grown in soil-filled rhizotrons and pots, the latter visualized by MRI (Fig. 1 *B* and *C* and *SI Appendix*, Fig. S1 *E–G*). Furthermore, the lateral roots arising from the seminal roots also displayed a highly increased growth angle (Fig. 1 *B* and *E* and *SI Appendix*, Fig. S1 *A* and *H*). Apart from the increased root growth angle, we did not detect any other aberrant root phenotypes, neither a changed number of seminal roots nor a difference in root length (*SI Appendix*, Fig. S1 *B* and *C*). To further investigate the reason for the steep root phenotype, we tested the responsiveness of the root system to gravity. After rotation by 90°, we monitored the angle of the root tips over time (Fig. 1 *F* and *G*). Roots of the *egt2-1* mutant bent much faster and stronger than wild-type roots, approaching 90° after 3 d compared to just 30° in wild-type roots (Fig. 1*G*). Root growth rate, however, was not altered (*SI Appendix*, Fig. S1*D*). We concluded therefore that the steep root angle of the *egt2-1* mutant was likely caused by a higher responsiveness to gravity. Since gravity sensing and signal transduction was shown to take place in the root cap and meristem (16–18), we compared the root cap and meristem by microscopy and measuring the root meristem size, but we did not discover significant differences (*SI Appendix*, Fig. S2 *A–D*). Other mutants with disturbed root gravitropism exhibit different velocities of starch granule settling in the root cap cells than wild type (19). However, we did not detect such differences between wild type and the *egt2-1* mutant (*SI Appendix*, Fig. S2 *E* and *F*).

Auxin Response Is Unaffected in *egt2-1* Mutants. It was shown before that the phytohormone auxin is involved in gravitropic response signaling (15) and that auxin transport inhibitors or external supply of auxin influences the reaction of roots to rotation (25). To analyze if the *egt2-1* mutant is sensitive to manipulation of the auxin state in the roots, we treated wild type and mutant with auxin and an auxin transport inhibitor and recorded the reaction to 90° rotation and root elongation in a time course experiment. Application of the naturally occurring auxin indole-3-acetic acid led to a similar gravitropic response and root elongation at low concentrations in both wild type and the *egt2-1* mutant compared to mock treatment (*SI Appendix*, Fig. S3 *A–D*) and to an inhibition of root growth and thereby a slower response to the gravistimulus at higher concentrations (*SI Appendix*, Fig. S3 *E* and *F*). Treatment with low concentrations of the auxin transport inhibitor 1-*N*-naphthylphthalamic acid (NPA) resulted in a similar gravitropic response and root elongation within 48 h in both wild type and *egt2-1* compared to mock treatment (*SI Appendix*, Fig. S3 *G–J*), while high concentrations of NPA decreased the gravitropic response and root elongation significantly in wild type and *egt2-1* to a similar degree compared to mock treatment (*SI Appendix*, Fig. S3 *K* and *L*). In summary, we demonstrated that *egt2-1* reacts to auxin treatment to the same degree as the wild type, and we conclude that the mutation in *egt2-1* does not disrupt the major auxin signaling pathways. This notion is consistent with the results of a tissue-specific RNA sequencing (RNA-seq) analysis of wild-type and *egt2-1* seminal roots, where we did not find any auxin-related genes among the differentially expressed genes (see *Results*).

***EGT2* Encodes a SAM Domain–Containing Protein.** In order to map and clone the *EGT2* gene, single nucleotide polymorphism-based bulked-segregant analysis (BSA) was carried out using an F_2-population derived from the cross between the hypergravitropic *egt2-1* carrying line TM2835 (in Morex background) and cultivar (cv.) Barke, the latter showing a typical wild-type, shallow root architecture. *egt2* was mapped to a 312 Mbp interval on the short arm of chromosome 5H (Fig. 2*A*) between markers *SCRI_RS_222345* and *SCRI_RS_13395* (Dataset S1). Subsequently, TM2835 was subjected to whole genome sequencing, which led to the identification of seven genes within the *egt2* interval and which carried missense, splice site, or stop-codon gain mutations when compared with wild-type Morex sequence (*SI Appendix*, Table S1). Among these was a gene encoding for a 252 amino acid SAM domain–containing protein [*HORVU5Hr1G027890* (26) or *HORVU.MOREX.r2.5HG0370880.1* (27)] with a mutation (G447A) leading to a premature stop codon at the beginning of the functional domain (W149*) (Fig. 2*B* and *SI Appendix*, Fig. S4 *A* and *B*) (27). Apart from the SAM domain, no other functional domains were predicted (28). The sequence of the SAM domain between EGT2, and previously described SAM domains of other plant species is highly conserved (*SI Appendix*, Figs. S4*B* and S6) (29, 30).

To validate *HORVU.MOREX.r2.5HG0370880.1* as *EGT2*, we used CRISPR/Cas9 to create an additional mutant allele (*egt2-2*) in the barley cv. Golden Promise. We targeted two sites in the 5' untranslated region (5′ UTR) and exon 1, separated by 196 bp, and recovered a 215 bp deletion including the start codon, leading to the translation of a truncated protein (Fig. 2*B* and *SI Appendix*, Fig. S4*A*). We analyzed the root phenotype of the homozygous T_1-line and determined a significantly higher root angle of both seminal and lateral roots in the mutant in comparison to the wild type (Fig. 2 *C–E*). Hence, we confirmed that the altered root angle phenotype of *egt2-2* is caused by a truncation of *HORVU.MOREX.r2.5HG0370880.1*. Like in the *egt2-1* mutant in Morex background, the root length of *egt2-2* was similar to the wild type (*SI Appendix*, Fig. S4*C*). The reaction of the *egt2-2* roots after rotation was faster than in the wild type but not statistically significant (*SI Appendix*, Fig. S4*E*). It is notable that Golden Promise and Morex differ in seminal root angle growth although they both carry a wild-type *EGT2* allele (compare Figs. 1 *A* and *D* and 2 *C* and *D*). Additionally, the reorientation of the roots after rotation occurs much faster in wild-type Golden Promise than in Morex (compare Fig. 1*G* and *SI Appendix*, Fig. S4*E*). Thus, other genetic factors influence the root growth angle in addition to *EGT2*.

To further validate the function of the *EGT2* gene, we identified mutant lines carrying premature stop codons from a sequenced mutant population of tetraploid wheat (31). We combined mutations in the two durum wheat *EGT2* orthologs (homologs on A and B genomes) to generate complete *egt2* knockout lines. These double mutants showed narrower seminal root growth angle in rhizoboxes compared with the sibling lines carrying wild-type alleles in both homologs (Fig. 2 *F* and *G*). Similar to barley, the number and length of seminal roots was unaffected in 7-d-old seedlings (*SI Appendix*, Fig. S4 *G–I*).

***EGT2* Is Expressed in the Whole Root Tip.** To survey the spatial expression patterns of *EGT2* in roots, we performed RNA in situ hybridization experiments. *EGT2* is expressed in the whole root tip, including the root cap, meristem, and elongation zone (Fig. 3*A*). The negative (sense) control exhibited background staining, mainly in the root cap; therefore, we confirmed this expression pattern by surveying our RNA-seq data, where we found *EGT2* expressed in

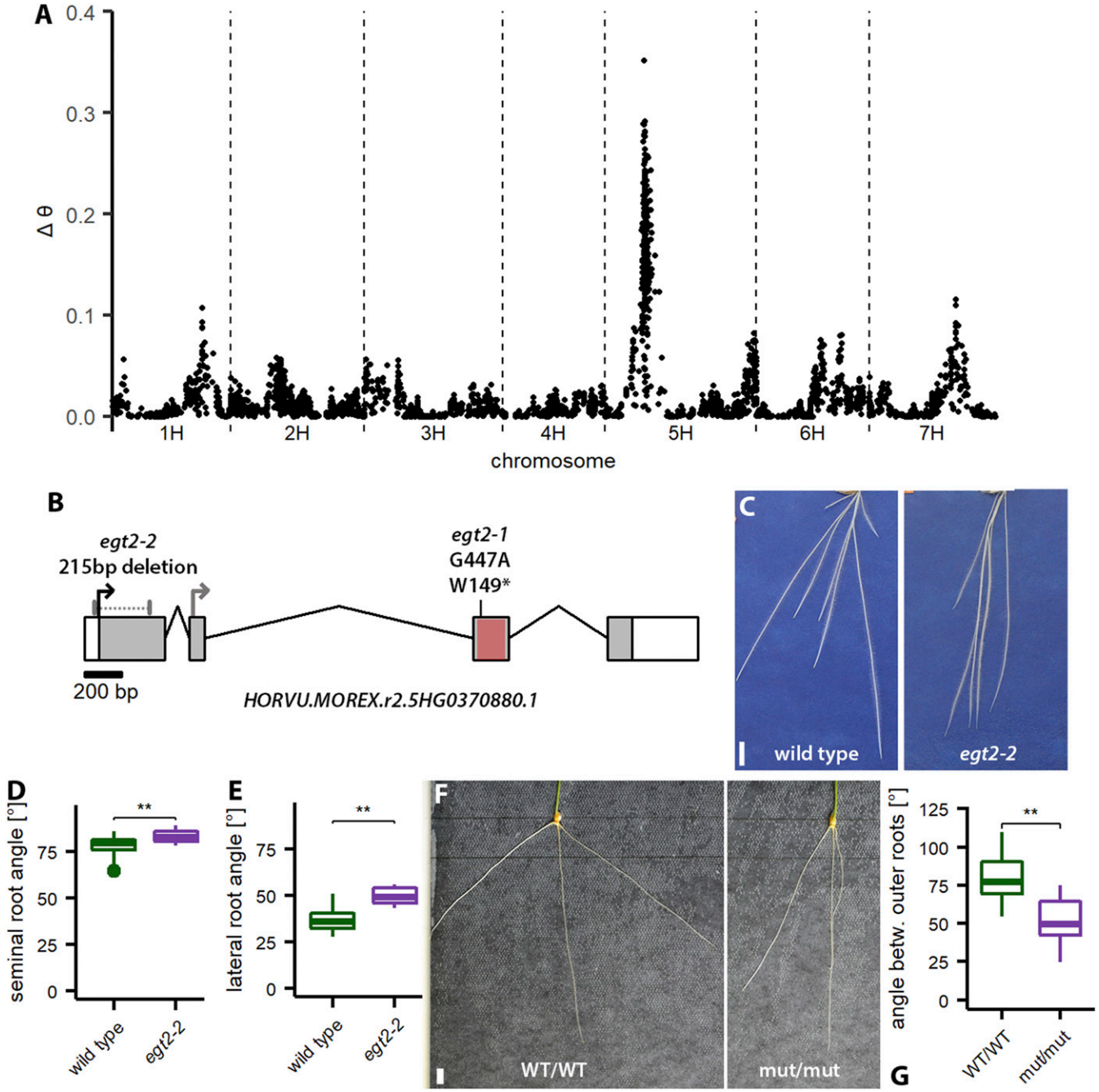

Fig. 2. *EGT2* encodes a SAM protein. (*A*) Association of SNP markers with seminal root angle across the barley genome as established by BSA in the F_2 cross TM2835 (*egt2-1,* hypergravitropic roots) × cv. Barke (wt roots). The *y*-axis reports $\Delta\theta$, an index accounting for the difference in allele-specific fluorescence signal between the two BSA DNA bulks, per SNP. (*B*) Gene structure of *EGT2* (HORVU.MOREX.r2.5HG0370880.1) with mutations in *egt2* (*egt2-1*: G to A transition and *egt2-2:* deletion); translational start site in wild type is shown as a black arrow and start site in the *egt2-2* mutant as a gray arrow; exons are depicted as a gray box, introns are depicted by lines, and UTRs are depicted as white boxes. The red box indicates the sequence encoding for the SAM domain. (*C*) Exemplary pictures of wild-type (cv. Golden Promise) and mutant *egt2-2* roots 7 DAG. (Scale bar: 2 cm.) (*D*) Seminal root angle of wild-type (cv. Golden Promise) and mutant *egt2-2* 7 DAG; $n = 15$ to 17 in two independent experiments. (*E*) Root angle of lateral roots 14 DAG; $n = 16$ to 18 in two independent experiments; two-tailed *t* test, $^*P < 0.05$, $^{**}P < 0.01$. (*F*) Exemplary pictures of wheat wild-type (WT/WT) and *egt2* (mut/mut) roots, 7 DAG. (Scale bar: 1 cm.) (*G*) Root angle between second and third seminal root of wild-type (WT/WT) and *egt2* (mut/mut) wheat seedling at 7 DAG; $n = 18$ and 39 for wild type and mutant, respectively. Wheat plants were derived from two independent segregating populations.

root cap, meristem, and elongation zone. qRT-PCR analysis of wild-type and *egt2* mutant root tips comprising root cap, meristematic, and elongation zone that were rotated by 90° for up to 9 h did not indicate any transcriptional regulation of *EGT2* with regard to gravistimulation (Fig. 3*B*). Furthermore, we measured *EGT2* expression in upper and lower flanks of the elongation zone 6 h after root rotation by 90° (Fig. 3*C* and *SI Appendix*, Fig. S5*A*) but did not detect any significant change. At all time points, *EGT2* expression was significantly down-regulated in the mutant, which is consistent which the observed premature stop codon in this gene likely leading to nonsense mediated decay of the transcripts (Fig. 3*B*). The control experiment with unrotated roots is depicted in *SI Appendix,* Fig. S8*B*.

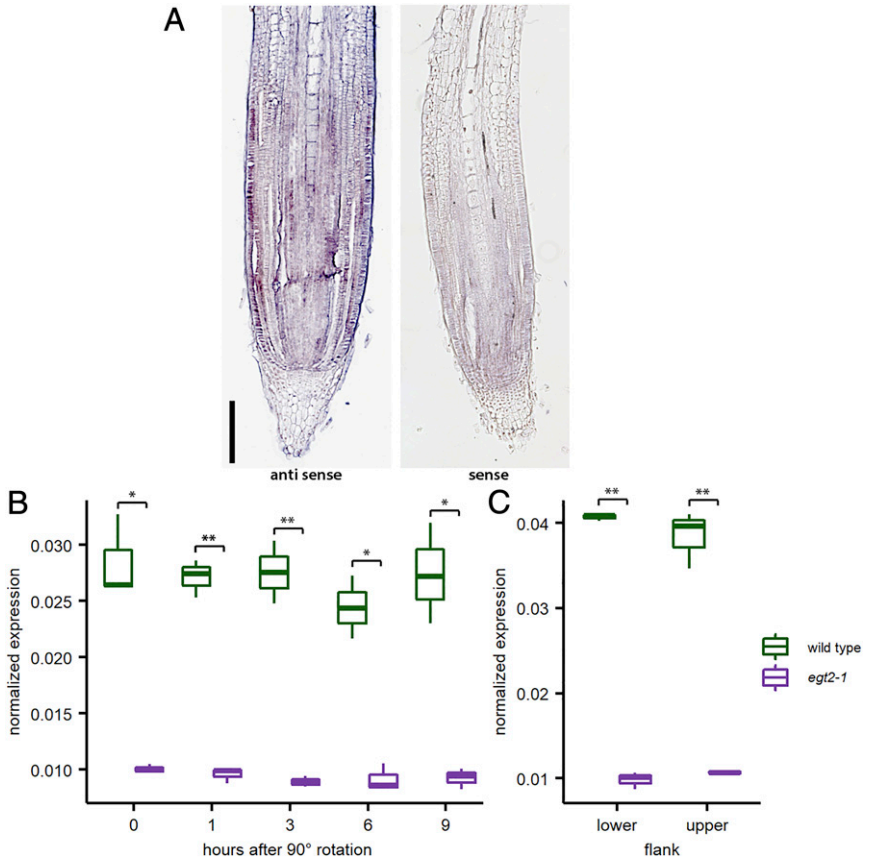

Fig. 3. Expression of *EGT2*. (*A*) RNA in situ hybridization of *EGT2*; negative controls (sense probes) are shown on the right. (Scale bar: 200 μm.) (*B*) qRT-PCR of *EGT2* expression in combined root cap, meristem, and elongation zone samples after rotation of 90°; normalized to *tubulin*; two-tailed *t* test, $*P < 0.05$, $**P < 0.01$. (*C*) qRT-PCR of *EGT2* expression in upper and lower flank of the elongation zone in roots after rotation by 90° for 6 h (as depicted in *SI Appendix*, Fig. S5*A*); normalized to *tubulin*; two-tailed *t* test, $**P < 0.01$.

In the *egt2-1* Mutant, Cell Wall–Related Processes Are Affected in the Elongation Zone. SAM domain–containing proteins from animals and plants have a plethora of different functions and act, among others, as transcription factors (29). To analyze the effect of the mutation in *EGT2* on the root transcriptome, we isolated RNA from different root tissues. For this, we applied laser capture microdissection to specifically separate root cap, meristem, and parts of the elongation zone from wild-type and *egt2-1* seminal roots. This allowed us to differentiate between gravity sensing (root cap), signal transduction (meristem), and signal execution (elongation zone) (Fig. 4*D* and *SI Appendix*, Fig. S5*B*). To this end, we selected the most vertically grown seminal roots in both genotypes that displayed a similar root growth angle (Fig. 4*A*). By doing so, we excluded secondary effects caused by different root growth angles. Moreover, we used roots of similar length to exclude differences in age since the barley seminal roots do not grow out simultaneously (32). The RNA-seq experiment yielded on average 41 million 100 bp paired-end reads per sample (*SI Appendix*, Table S2). We determined the transcriptomic relationships among the two genotypes and three tissues by a principal component analysis (PCA) (Fig. 4*B*). In the PCA, the two principal components PC1 and PC2 explained 82% of the total variance (Fig. 4*B*). The biological replicates per tissue included four wild-type and four mutant samples clustering closely together. This indicates small transcriptomic differences between the genotypes but large differences between the tissues. To identify differentially regulated genes, we computed pairwise contrasts between the genotypes of the respective tissues (false discovery rates [FDR] <5% and $\log_2$FC >|1|; see *Materials and Methods*) for genes that uniquely mapped to chromosomes 1 to 7 (33). This resulted in 67 differentially regulated genes among all tissues, some of which were shared between all or two tissues (Fig. 4*C* and *SI Appendix*, Fig. S7 and Table S3). Strikingly, we found seven genes encoding for expansins down-regulated in the elongation zone of the mutant *egt2* (*SI Appendix*, Figs. S7 and S8*A*). Among them, *HORVU3Hr1G076620* and *HORVU3Hr1G076650* are highly homologous, with a sequence identity of 99.5%. A time course experiment with the other five of these expansins did not display expression differences between wild type and *egt2* upon rotation of the roots by 90° (*SI Appendix*, Fig. S8 *C*–*G*). Gene ontology (GO) terms were only assigned to genes down-regulated in the elongation zone, all of them related to the term cell wall (Fig. 4*E*). At the same time, this validates our data set since expansins are expressed in the elongation zone and differentiated root tissue (34). Furthermore, we found that several genes categorized as peroxidase superfamily protein members were up-regulated in either the meristem or the elongation zone (*HORVU2Hr1G026420*, *HORVU7HR1G020300*, *HORVU3Hr1G036820*) (*SI Appendix*, Fig. S7). Differential regulation of a peroxidase superfamily protein-encoding gene was already found in a study in *Arabidopsis* related to agravitropic mutants (35). Moreover, we demonstrated that a gene encoding for calmodulin, a primary plant calcium receptor, down-regulated in meristem and elongation zone (*HORVU1Hr1G068440*) (*SI Appendix*, Fig. S7). Finally, we identified a gene annotated as exocyst complex component 7 up-regulated in the meristematic zone. Components of the exocyst are involved in directing exocytotic vesicles to fusion sites on the plasma membrane and might be involved in the distribution of the auxin transporter PINFORMED4 in *Arabidopsis* (36, 37).

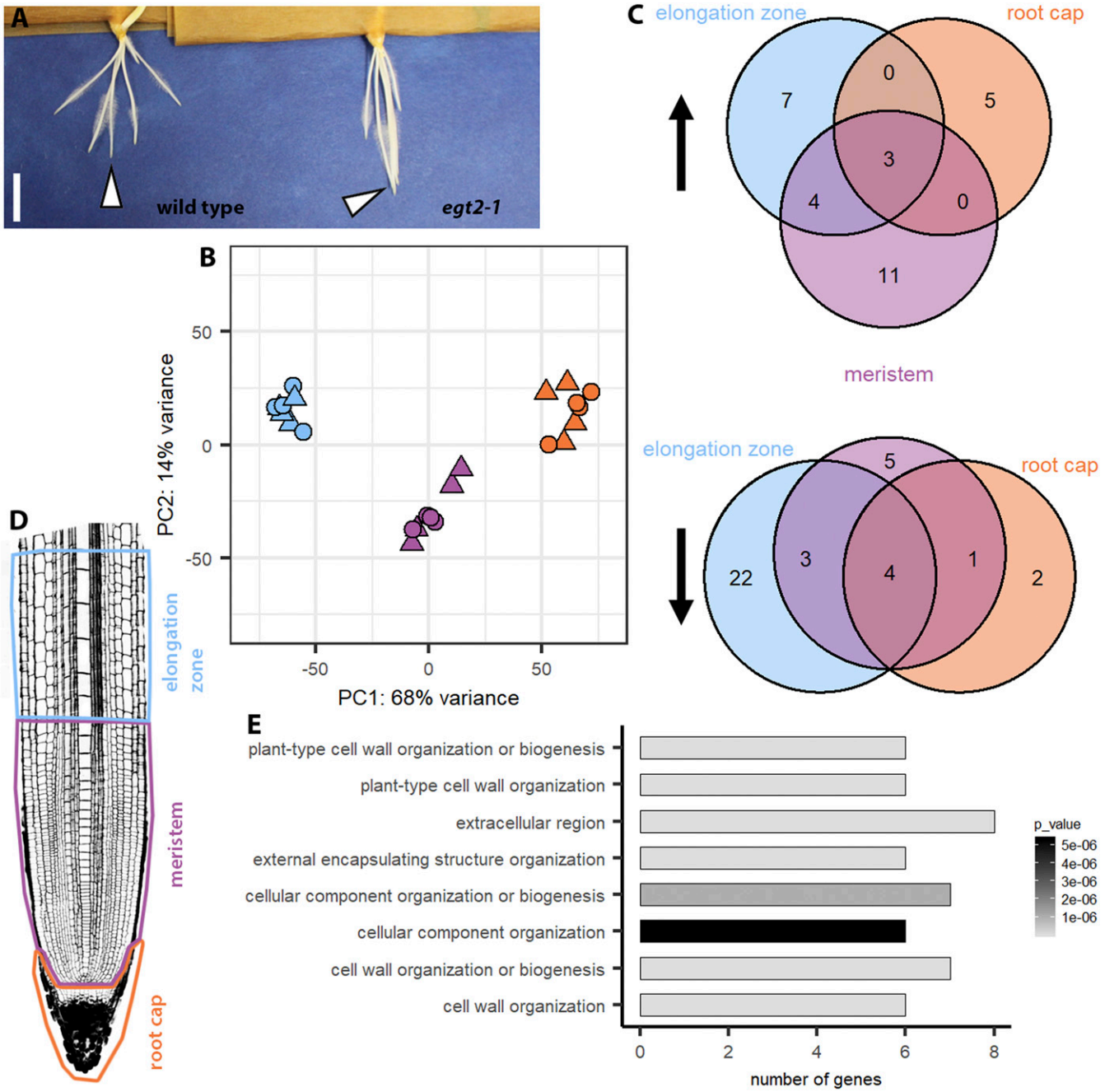

Fig. 4. RNA-seq reveals differences in cell wall-related processes in the elongation zone. (*A*) Wild-type and *egt2-1* plants 3 DAG used for RNA isolation. (Scale bar: 1 cm.) Arrow heads point to exemplary roots used for RNA isolation (most vertical ones). (*B*) PCA of the 24 RNA-seq samples of the two genotypes and three tissues; first and second principal components collectively explain 82% of the variance. (*C*) Venn diagram showing up-regulated (upward arrow) and down-regulated (downward arrow) differentially expressed genes (DEGs) in the respective tissue. (*D*) Experimental setup: RNA of root cap, meristem, and 900 μm of the elongation zone were isolated. (*E*) Enriched GO terms for DEGs down-regulated in the elongation zone.

Discussion

The optimization of root system architecture has been recognized as one of the most important objectives in current breeding programs aimed at increasing resilience and sustainability of crops and agricultural systems (4, 38). Variation of root growth angle can affect the way roots anchor to and explore different soil layers and capture nutrients and water and thus can influence drought tolerance, as shown for DRO1 in rice (4). Specifically, modeling and experimental evidence showed that steeper root angle growth can increase root system depth, thus helping plants in foraging for water and mobile nutrients, such as nitrogen (3–6). Possible tradeoffs are inefficient acquisition of less mobile, superficial nutrients such as phosphate or increased susceptibility to waterlogging and salinity (3, 39). Steeper root system is also expected to reduce the total volume of soil explored, alter intra- and interplant root competition, and contribute to root lodging, although these effects are strongly interconnected with crop management factors such as seeding rate (3, 40, 41). However, knowledge about genes, gene interactions, and regulatory networks in root development is currently limited in all major crops, including cereals.

Here, we cloned a key regulator of root gravitropism, *ENHANCED GRAVITROPISM2* (*EGT2*), in barley and wheat. Mutations in *EGT2* lead to enhanced gravitropic response and thereby to a steeper root growth angle of seminal and lateral roots. We did not find any other root or shoot morphological trait affected by this mutation, indicating that *EGT2* does not act in an ubiquitous signaling pathway but rather is specific for root gravitropism. In *Arabidopsis*, most gravitropic mutants were discovered because they show agravitropic root phenotypes (20, 42). In grasses, however, some mutants with hypergravitropic roots were discovered, for instance, *vln2* and *rmd*. The villin protein VLN2 facilitates microfilament bundling, while the actin-binding protein RMD links actin filaments with gravity-sensing organelles (19, 25).

The only predicted domain in EGT2 is the SAM domain. In animals, SAM domain–containing proteins function as transcription factors, receptors, kinases, or ER proteins (29). In plants, the best known protein containing a SAM domain is the transcription factor LEAFY (LFY), which is involved in flower and meristem identity formation. Modeling of *Arabidopsis* SAM proteins based on structure predictions and LFY characterization suggests that the majority of these proteins are able to form head-to-tail homo- or hetero-oligomers/polymers (29). The close phylogenetic relationship of EGT2 with AtSAM5 (At3g07760) indicates a similar potential of oligomerization for EGT2.

EGT2 is also closely related to WEEP, a SAM domain containing protein that was discovered because of the prominent shoot phenotype in peach tree mutants (30). Peach trees with deletions in *WEEP* show a weeping shoot growth phenotype; thus, the branches grow in a wider angle, and after gravistimulation by rotation by 90°, the branches do not orient their growth upward again (30). Therefore, EGT2 and WEEP are likely involved in a similar pathway that regulates gravitropism, but in different plant organs. Bud grafting experiments in peach implied that *WEEP* encodes an autonomous determinant of shoot orientation for each branch and that no mobile signals from other parts of the plants (like phytohormones) are necessary (30). Furthermore, no difference of auxin or abscisic acid concentration was detected in growing shoots between peach wild-type and *WEEP* mutants, nor were genes associated with auxin biosynthesis or perception differentially expressed (30).

Similarly, we did not find any expression changes of genes related to auxin biosynthesis or perception in our transcriptomic comparison between wild type and *egt2-1*. Treatments with auxins or an auxin transport inhibitor confirmed that the *egt2-1* mutant is as sensitive to disturbance of the auxin balance as the wild type (*SI Appendix*, Fig. S3), indicating that EGT2 works independently of auxin. Nevertheless, the auxin transport pathway could still be affected, as demonstrated for the rice mutant *villin2* (*vln2*) that exhibits a disturbed recycling of the auxin efflux carrier PIN-FORMED2 (PIN2) and thereby a hypergravitropic root response (25). However, auxin treatment of *vln2* mutants induced a restoration of the phenotype and the mutants were insensitive to auxin transport inhibitors which differs from *egt2-1*. On the other hand, exocyst complex component 7 was transcriptionally up-regulated in the *egt2-1* mutant. In *Arabidopsis*, disturbing the expression of *EXOCYST70A3* by knockout or overexpression leads to a higher agravitropic response upon auxin efflux inhibitors probably by regulating the PIN4 localization in columella cells and thereby auxin distribution in root tips (37). It is conceivable that disturbance of expression levels in *egt2-1* mutants might lead to a change in PIN localization and thereby a changed signal transduction; however, this hypothesis remains to be tested. The ubiquitous expression of *EGT2* in root cap, meristem, and elongation zone suggests a participation rather in the signal transduction of gravitropism than in the sensing or differential cell elongation. Since the *EGT2* expression does not change upon gravistimulus, neither in expression level nor in distribution, signal transduction most likely occurs on protein level.

In a split-ubiquitin yeast two-hybrid screen, the close homolog of EGT2, AtSAM5 interacted with the calcium-dependent protein kinase AtCPK13 (At3G51850) (43), putatively connecting AtSAM5 to calcium signaling pathways. Inhibition of the primary plant calcium receptor calmoldulin was shown to inhibit the response to gravity in *Arabidopsis* (42). In the *egt2-1* mutant, *Calmodulin 5* is transcriptionally down-regulated in the meristem and elongation zone, putatively connecting EGT2 with calcium-dependent signal transduction. It is still generally unknown, however, which role calcium plays in gravitropic signaling.

If we hypothesize a role for EGT2 in signal transduction, we would expect downstream targets in the elongation zone, where the effect of gravity sensing is executed by differential cell elongation (18). Here, we found a striking number of expansin genes transcriptionally down-regulated (*SI Appendix*, Fig. S7). Expansins are known as acid-induced cell wall loosening enzymes. However, most studies are based on the activity of bacterial enzymes and the function of expansins in plant cell walls is still unknown (34). Similarly, cell wall-related genes are differentially regulated in *weep* mutant peach trees, and the differentially regulated auxin response genes in *weep* mutants have roles in mediating cell expansion, or modulation of H^+ transport (30). Besides expansins, we found three genes encoding peroxidase superfamily proteins up-regulated in the meristem and elongation zone (*SI Appendix*, Fig. S7). Down-regulation of a peroxidase superfamily protein-encoding gene was already demonstrated in a study in *Arabidopsis* comparing inflorescence stems of wild type to *scarecrow* and *short root* mutant transcriptomes, which show no gravitropic response to rotation in the shoot (35). Peroxidases catalyze the consumption or release of H_2O_2 and reactive oxygen species (ROS). One class of peroxidases functions extracellularly, either for cell wall loosening or cell wall cross-linking (44), and the transcriptional regulation in *egt2* might be related to the regulation of the expansins. Moreover, it was shown that ROS work downstream of auxin signaling in root gravitropism, maybe as second messenger (45).

Based on the broad expression pattern of *EGT2* throughout root cap, meristem, and elongation zone, and the interaction of the *Arabidopsis* AtSAM5 homolog with CPK13, we can hypothesize that *EGT2* is involved in the signal transduction of gravitropic signaling. The missing interference in auxin-related processes on the transcriptomic level and the susceptibility to auxin treatments implies that EGT2 is not involved in any signal transduction related to changes in auxin levels and/or transport. It is possible that EGT2 acts in a pathway that counteracts the auxin-mediated positive gravitropic signaling pathway, since for the growth in an angle toward the gravity vector, a pathway counteracting the positive reaction to gravity is needed. By knocking it out, the downward growth of the roots would dominate and create the hypergravitropic phenotype.

In summary, our results suggest that *EGT2* is an evolutionary conserved check point of seminal and lateral root growth angle in barley and wheat. *EGT2* could be a promising target for root-based crop improvement in cereals.

Materials and Methods

Plant Material and Growth Conditions. The *egt2-1* mutation carrying line, TM2835, was derived from sodium-azide mutagenesis of the cv. Morex as previously described (23, 24). For growth in rhizoboxes and on agar plates, the seeds were washed in 1.2% sodium hypochlorite for 5 min and rinsed with distilled water. Then they were incubated in darkness at 30 °C overnight to induce germination and only germinating seeds were used for further experiments. Growth in rhizoboxes for plant phenotyping and rotation experiments were conducted as described before (46). For phytohormone treatments, plants were grown on half-strength Hoagland solution (47), pH 5.8, supplemented with 0.8% phytagel on square Petri dishes, which were placed at a 45° angle. The plants were grown in growth cabinets (Conviron) at 18 °C at night (8 h) and 22 °C at day (16 h). For growth in

rhizotrons filled with peat substrate, wild-type and *egt2* mutants were grown in the GrowScreen-Rhizo automated platform for 24 d as previously described (48). For the MRI measurements, the seeds were placed in a Petri dish on wet filter paper. The Petri dish was sealed with parafilm and stored lightproof for 24 h in the growth chamber (16 °C/20 °C night/day temperature, 14 h light per day) to induce germination and only germinated seeds were used for further experiments. Seeds were subsequently sown in field soil (Sp2.1, Landwirtschaftliche Untersuchungs- und Forschungsanstalt). Soil moisture was kept at 8.9%$_{m/m}$, corresponding to 40% of the maximal water holding capacity (49). Per genotype, 18 seeds were planted in one pot (Ø = 12.5 cm, 12 cm height) in a hexagonal grid with 2.5-cm seed spacing. Seedlings were imaged after 3 d in the growth chamber. For a longer experiment, single seeds were planted into larger pots (Ø = 9 cm, 30 cm height) and were grown for one week before imaging.

Durum wheat (*Triticum turgidum*) *egt2* mutants were identified from a TILLING population developed in tetraploid cv. Kronos (31). Two selected lines (Kronos2138 and Kronos3589) carrying premature termination codons in the two *EGT2* homeologous coding sequences (TraesCS5A01G102000 and TraesCS5B02G164200LC) were crossed and F_1 plants were self-pollinated. Progenies of selected wild-type and double mutant F_2 individuals derived from two independent initial crosses were grown in rhizoboxes for seminal root angle analysis. Seeds were washed in 70% ethanol for 1 min, then in 1% sodium hypochlorite + 0.02% TritonX-100 for 5 min and rinsed with distilled water. Sterilized seeds were pregerminated for 24 h at 28 °C in wet filter paper. Only germinating seeds were transferred in rhizoboxes for 7 d at 25 °C.

Phenotyping Experiments and Rotation Tests. For analysis of the root angles, plants were grown in rhizoboxes for 7 (seminal root angle) or 14 d (lateral root angle). The seminal root angle was measured as angle from the shoot to the root tip, in relation to the horizontal. For the angle of the lateral roots, the angle was measured from the outgrowth point of the main root to the lateral root tip in comparison to the horizontal. Twenty randomly chosen lateral roots were measured per plant. For the rotation tests, the plants were grown in rhizoboxes for 5 d and then rotated once by 90°. For phytohormone treatments, the plants were grown for 5 d on agar without phytohormones and then transferred to agar plates supplemented with phytohormones as indicated in the results. After 1 h recovery, the agar plates were rotated once by 90°. Pictures were taken at the time points indicated in the graphs. For analysis, the root angle of every single root tip was measured in relation to the horizontal and the angle right after rotation was set to 0. For all measurements, the average of all roots per plant was calculated, presented in the graphs, and compared in the statistical tests. For analysis of growth in the rhizotrons, root images were collected every 2 d, enabling to distinguish between seminal and crown roots. Images at 24 d were utilized for seminal, nodal, and lateral root angle analysis. Root angle values were collected with the software ImageJ (50).

RNA In Situ Hybridizations. Probes for *EGT2* (HORVU5Hr1G027890) mRNA were prepared from the whole coding sequence (start to stop codon). Cloning and RNA probe synthesis was performed as described before (32). RNA in situ hybridizations on roots of 7-d-old plants were performed as described before (32).

BSA and Whole Genome Sequencing. BSA (51) was carried out using plants from an F_2-population obtained starting from the cross TM2835 × cv. Barke and segregating for the *EGT2* locus. 106 F_2-seedlings were grown in flat rhizoboxes composed by two black plastic panels of 38.5 × 42.5 cm. Five pregerminated seeds (1 d, 20 °C, on wet filter paper, in the dark) were positioned between moist filter paper sheets within each rhizobox. Each rhizobox was placed vertically in a larger plastic tank containing deionized water to a level of 3 cm from the bottom, in growth chamber) at 18 °C at night (8 h) and 22 °C at day (16 h) for 13 d. At the end of the growing period, root growth angle of seedlings was visually evaluated and a segregation rate of 88:18 (wild type vs. hypergravitropic) recorded confirming that *egt2* segregates as a monogenic recessive Mendelian locus (χ^2 3:1 = ns). Immediately after this inspection, 15 plants showing wild-type root growth angle and 15 plants showing an hypergravitropic angle were chosen for DNA preparation on a single plant basis using 2 cm^2 leaf portions as previously described (23). DNA samples for BSA were obtained by mixing equal DNA amounts of each of the 15 bulk components, to a final concentration of 50 ng/ul. The two DNA bulks (in double) along with single plant DNA samples from 10 hypergravitropic plants were genotyped using the 9k Illumina Infinium iSelect barley SNP array (52). SNPs signal was analyzed using GenomeStudio (Illumina, San Diego, Inc.). For DNA bulks, SNPs signal was interpreted using the theta value approach as described in ref. 53, modified in order to integrate for each SNP the signals obtained from two bulks (wild type or $^{+/+}$ and hypergravitropic or $^{-/-}$) in the "delta theta" value score as follows "delta theta" = [(theta bulk$^{+/+}$)-(theta bulk $^{-/-}$)]^2.

Genomic DNA of TM2835 for whole genome shot gun sequencing was extracted from leaf samples using a commercial kit (Macheray-Nagel Nucleospin Plant II). The DNA was sequenced with Illumina HiSeq PE150, and 699,353,963 paired-end reads were produced corresponding to a coverage of approximately 40×. Reads were aligned to the first version of barley cv. Morex reference genome (26) with BWA v.7.12 (54) and variants in the genomic space were called with SAMtools v. 1.3 (55, 56), filtering for a minimum reads depth of 5×, PHRED quality >40. In order to discard background mutations due to the differences between the official Morex reference and the Morex parental seeds which had previously been used in the mutagenesis, the SNP calling considered further eight TILLMore mutants whole genome sequencing data that was available at that moment, filtering with a custom AWK script for a minimum ratio DV/DP of 0.8 for the *egt2* mutant and a maximum ratio of 0.2 in every other mutant, where DP is the coverage depth at the SNP position and DV is number of nonreference bases at the same position. SNP effects were predicted with SNPEff v.3.0.7 (57).

For coverage analysis, a minimum of 5× read depth was considered, resulting in a target region of 3.5 GB containing a total of 15,805 mutations, hence the estimated mutation load on the entire genome is 22,579 mutations, or approximately 1 mutation per 220 kb which is of the same order of magnitude of mutation density (1 per 374 kb) formerly estimated based on TILLING results from the same TILLMore population (23). For the provean analysis, values <−2.5 were considered deleterious and values >−2.5 were tolerated.

Modified Pseudo-Schiff Propidium Iodide and Lugol's Staining. The modified pseudo-Schiff propidium iodide staining was performed as described in ref. 32. For Lugol's staining, roots were fixed in 4% paraformaldehyde in phosphate-buffered saline (PBS) overnight, embedded in 13% agarose and sectioned at the vibratome with 40-μm thickness. Then, they were stained with Lugol's solution for 3 min and rinsed with PBS buffer.

Amyloplast Sedimentation Rate. After 1-d pregermination, wild-type and *egt2-1* plants were grown in rhizoboxes for 7 d and then rotated by 180° (shoots pointed downwards). The 0.5 cm root segments of the root tips were collected before rotation and 1 min, 2.5 min, 5 min, and 10 min after rotation. Eight plants were used for each genotype at each time point. Samples were fixed immediately in 4% PFA (diluted with PBS from 36% formaldehyde, VWR Chemicals), and placed in vacuum for 10 min. Subsequently, the solution was replaced and the samples were swirled at 4 °C overnight. Then, the fixed root samples were embedded in 13% low-melting agarose (peqlab) and sectioned longitudinally in a vibratome (Leica Biosystems) with a thickness of 40 μm. Root sections were stained with Lugol's solution (Roth) for 3 min and washed with PBS buffer, and pictures were taken with a light microscope (Zeiss).

Images of root sections were analyzed by ImageJ. The distance from the center of statoliths to the former distal cell wall and new lower cell wall were measured, respectively. Ten cells in the center of each root section were measured and the data of cells with a length of 25 μm to 40 μm were used for graphing.

Microscopy. RNA in situ hybridization and Lugol's-stained samples were examined using a Zeiss PALM MicroBeam microscope.

MRI. MRI images were acquired on a 4.7 T vertical magnet equipped with a Varian console (58). A multislice spin echo sequence was used. Sequence parameters were adapted to the different pot sizes. For the 9 cm pots, we used a birdcage RF coil with a 10 cm diameter and the following sequence parameters: 0.5 mm resolution, 1-mm slice thickness, 9.6 cm field of view, TE = 9 ms, TR = 2.85 s, Bandwidth = 156 kHz, two averages. For the 12.5 cm pots, the following parameters were changed: birdcage RF coil with 140 mm diameter, 14 cm field of view, and 0.55 mm resolution.

CRISPR. For CRISPR target sequences, we choose 20 base pair sequences with the protospacer adjacent motif PAM sequence NGG in the first exon of *EGT2* (HORVU5Hr1G027890) that we checked at http://crispr.dbcls.jp/ for off-targets in the barley genome (Barley [*Hordeum vulgare*] genome, 082214v1 [March 2012)]. We used sites with only one predicted target for a 20mer and only up to 3 predicted targets for the 12mer target sequence upstream of the PAM. The CRISPR guide sequences are marked in *SI Appendix*, Fig. S4*A*. The sgRNA shuttle vectors pMGE625 and 627 were used to generate the binary vector pMGE599 as described in ref. 59. Transformation was carried out with the spring barley cv. Golden Promise grown in a climate chamber at 18 °C/14 °C (light/dark) with 65% relative humidity, with a 16 h photoperiod and a photon

flux density of 240 μmol · m^{-2} · s^{-1}. The binary vector pMGE599 was introduced into *Agrobacterium tumefaciens* AGL-1 strain (60) through electroporation (*E. coli* Pulser; Bio-Rad). The scutella tissue of barley caryopsis was used for *Agrobacterium*-mediated transformation as described previously (61). The insert integration in the barley genome was confirmed by detection of hygromycin gene sequences via PCR in generated T0 lines and were analyzed for mutations in *EGT2* by PCR and Sanger sequencing and the seeds for T1 generation were used for experiments.

qRT-PCR. For the qRT-PCR, RNA from plants grown for 7 d after germination in rhizoboxes was extracted with the RNeasy Plant Mini Kit (Qiagen) and first strand complementary DNA (cDNA) was synthesized with the RevertAid First Strand cDNA Synthesis Kit (Thermo Fisher). Four plants were pooled per biological replicate, and samples were taken from the root tip containing the meristematic and elongation zone, ∼2 mm until the outgrowth of root hairs. For each genotype, three biological replicates and three technical replicates were used. For the reaction, 2 μL of PerfeCTa SYBR Green SuperMix (Quantabio), 1 μL primer mix of a concentration of 1 μM, and 1 μL cDNA was mixed. The primer efficiency of each oligonucleotide was calculated using the following dilution series: 1, 1/2, 1/4, 1/8, 1/16, 1/32, 1/64, and 1/128. The relative expression levels of the transcripts were calculated with reference to the housekeeping gene *TUBULIN* (*HORVU1Hr1G081280*) and according to the method described in ref. 62. Oligonucleotide primer sequences are listed in *SI Appendix*, Table S4. Significant differences in gene expression levels were determined by a two-sided Student's *t* test.

Laser Capture Dissection Microscopy and RNA-Seq. Root tips of the most vertically grown seminal root of 3-d-old plants were used and assigned as one biological replicate. Per genotype, four biological replicates were analyzed. Plants were grown in rhizoboxes and fixed with Farmer's fixative (EtOH:acetic acid 3:1) on ice for 15 min under 500 mbar vacuum and subsequent swirling at 4 °C for 1 h. The fixation solution was replaced, and the procedure was repeated twice before replacing the solution with 34% sucrose and 0.01% safranin-O in PBS. The samples were vacuum-infiltrated again for 45 min and incubated on ice at 4 °C for 21 h. Then the samples were dried carefully with tissue paper and embedded in tissue-freezing medium as described before (63). The medium blocks containing the tissue were stored at −80 °C and were acclimatized to −20 °C in the cryomicrotome (Leica CM1850). Longitudinal sections of 20-μm thickness were mounted on poly-L-lysine-coated glass slides (Zeiss), and the tissue-freezing medium was removed after 5:30 min by incubation in 50% EtOH and 1 min incubation each in 70% EtOH, 95% EtOH, 100% EtOH, and 100% xylol (RNase-free). The tissues (root cap, meristem, and 900 μm of the elongation zone adjacent to the meristem, *SI Appendix*, Fig. S5*B*) were cut with the following settings of the PALM Microbeam laser capture instrument (Zeiss, Germany): energy: 79; speed: 100; cutting program: "Center RoboLPC," picked up manually with a sharp needle and transferred to the cap of RNase-free adhesive caps (Zeiss). RNA was isolated with the Arcturus PicoPure RNA Isolation Kit (Thermo Fisher) according to the manufacturer's protocol for tissue, including the DNase treatment. RNA quality was determined with an Agilent 2100 Bioanalyzer using the Agilent RNA 6000 Pico kit and yielded RIN values between 7.1 and 8.9 and a concentration between 610 and 95,000 pg/μL. Preamplification and library preparation was carried out as described in ref. 64. Detection and sequencing were performed on an Illumina NovaSeq sequencing instrument with a PE100 protocol. Trimmomatic version 0.39 (65) was used to remove low-quality reads and remaining adapter sequences from each read dataset. Specifically, a sliding window approach was used, in which a read was clipped if the average quality in a window of 4 bp fell below a phred quality score of 15. Only reads with a length of ≥30 bp were retained for further analyses. Data are deposited at the sequence read archive (SRA), PRJNA589222. BBDuk of the BBTools suite (https://jgi.doe.gov/data-and-tools/bbtools/) was employed to remove rRNA reads from the datasets using a kmer length of 27 as a filtering threshold for decontamination. After removal of rRNA reads, on average, 8 million paired reads remained. The splice-aware STAR aligner v.2.7.2b (66) was used to align the remaining reads against a genome index of the barley reference sequence and annotation of genotype Morex (IBSC v2.0) (26). Multimapping reads that mapped to more than one position were excluded from subsequent steps by considering only reads, which mapped in a single location (–outFilterMultimapNmax 1). On average, 5 million reads per sample aligned to unique positions in the gene set of the IBSC v2.0 barley reference genome with 46,272 predicted coding and noncoding gene models [EnsemblPlants release 45 (26)]. The aligned paired-end reads were ordered according to their position and transformed to .bam files by the software SAMtools [version 1.3.1 (55)]. Alignment of sequences to the reference genome of Morex (release 45) (26) was performed using HTSeq [version 0.10.0 (67)] with the parameters "-r pos -i gene_id -s no–secondary-alignments ignore–supplementary-alignments ignore." The PCA was performed on the expression data using the normalization procedure rlog() implemented in the R package DESeq2 and the plotPCA() function [version 1.22.2 (33)]. Expression values were normalized with library size by calculating fragments per million (FPM) reads using the fpm() function of DESeq2, after removal of lowly expressed genes with less than 10 reads over all samples. Expression levels of genes were estimated by the variance-mean dependence in the count table based on a generalized linear model using the negative binomial distribution within the R package DESeq2 (33) calculating $\log_2$ fold change ($\log_2$FC) values between wild type and mutant in the respective tissues with the design ∼ genotype + tissue + genotype:tissue. Significance values for $\log_2$FC values were calculated as Wald test *P* value and were adjusted by the Benjamini-Hochberg procedure to obtain FDR (68). Genes with an FDR <5% and $\log_2$FC >|1| were considered differentially expressed. From this gene set, we excluded gene pairs that were assigned to chr0 and chr1, which had the same annotation, and the respective gene partner was the one with the closest related transcript after a BLAST search. GO term enrichment of the resulting gene set was performed using agriGo (69). The sequencing data have been deposited in the National Center for Biotechnology Information sequencing read archive (PRJNA589222).

Laser Capture Dissection Microscopy for Separating the Upper and Lower Flanks of Roots. Laser capture dissection microscopy was used to separate cells for the analysis of gene expression levels in the upper and lower flanks of rotated roots (*SI Appendix*, Fig. S5*A*). Six hours after rotating 7-d-old plants grown in rhizoboxes by 90°, 5-mm-long root tip segments of the initially most vertical roots were collected and then fixed, embedded, and sectioned as described. The cortical and epidermal cells of 1.5 mm of the elongation zone adjacent to the meristem were cut by a PALM Microbeam Platform (Zeiss) with the following settings: energy: 54; speed: 3; and cutting program: "Cut," picked up manually with a sharp needle and transferred to the cap of RNase-free adhesive caps (Zeiss).

RNA was isolated and analyzed as described. RIN values of RNAs were between 6.7 and 7.8, and concentrations were between 9 and 20 ng/μL. RNA of three roots from independent plants was used as one biological replicate; three biological replicates were analyzed for each genotype and flank.

Phylogenetic Analysis. The EGT2 (HORVU.MOREX.r2.5HG0370880.1) protein sequence was BLASTed on Phytozome v12.1 to the *Brachypodium dystachyon* proteome v3.1, the *Oryza sativa* proteome v7_JGI, the *Zea mays* proteome Ensembl-18, the *Arabidopsis thaliana* proteome TAIR10, the *Prunus persica* proteome v2.1, and the *Sorghum bicolor* proteome v3.1.1 with the default settings. Hits with E-values <3.9×10^{-77} were considered. The identified orthologs were then confirmed using the EnsemblPlants Compara Ortholog tool. Retrieved protein sequences were aligned by ClustalW in the software MEGA X, with default values (70): Ancestral states were inferred using the maximum likelihood method (71) and JTT matrix-based model (72). The tree shows a set of possible amino acids (states) at each ancestral node based on their inferred likelihood at site 1. The initial tree was inferred automatically by applying Neighbor-Join and BioNJ algorithms to a matrix of pairwise distances estimated using the JTT model and then selecting the topology with superior log likelihood value. The rates among sites were treated as being uniform among sites (Uniform rates option). This analysis involved 16 amino acid sequences.

Data Availability. RNA-seq data have been deposited in SRA (https://www.ncbi.nlm.nih.gov/bioproject/PRJNA589222).

ACKNOWLEDGMENTS. This work was funded by the Deutsche Forschungsgemeinschaft Grant HO2249/21-1 (to F.H.). K.A.N., D.P., and R.K. acknowledge support from the Helmholtz Association for the Forschungszentrum Jülich. The rhizotron study received funding from the European Union's Horizon 2020 research and innovation program under Grant Agreement No. 731013 (EPPN2020). Work described here is supported in part by the project "Rooty: A root ideotype toolbox to support improved wheat yields" funded by the IWYP Consortium (Project IWYP122) to C.U., J.S., R.T., and S.S. via the Biotechnology and Biological Sciences Research Council in the United Kingdom (BB/S012826/1). We thank Felix Frey (University of Bonn) for his advice on RNA-seq data analysis and discussion, Johannes Stuttmann (University of Halle) for sharing the CRISPR/Cas cloning vectors, and Shalima H. Orse for support throughout the project. We thank Anna Galinski, Jonas Lentz, Carmen Müller, Bernd Kastenholz, Ann-Katrin Kleinert, Roberta Rossi, and Kwabena Agyei (Forschungszentrum Jülich GmbH) for their assistance during the rhizotron study. R.K. and D.P. gratefully acknowledge Dagmar van Dusschoten and Johannes Kochs for support and maintenance of the MRI System.

1. T. Wheeler, J. von Braun, Climate change impacts on global food security. *Science* **341**, 508–513 (2013).
2. N. Ramankutty *et al*., Trends in global agricultural land use: Implications for environmental health and food security. *Annu. Rev. Plant Biol.* **69**, 789–815 (2018).
3. J. P. Lynch, Root phenotypes for improved nutrient capture: An underexploited opportunity for global agriculture. *New Phytol.* **223**, 548–564 (2019).
4. K. P. Voss-Fels, R. J. Snowdon, L. T. Hickey, Designer roots for future crops. *Trends Plant Sci.* **23**, 957–960 (2018).
5. Y. Uga *et al*., Control of root system architecture by DEEPER ROOTING 1 increases rice yield under drought conditions. *Nat. Genet.* **45**, 1097–1102 (2013).
6. A. P. Wasson *et al*., Traits and selection strategies to improve root systems and water uptake in water-limited wheat crops. *J. Exp. Bot.* **63**, 3485–3498 (2012).
7. R. Tsugeki, N. V. Fedoroff, Genetic ablation of root cap cells in *Arabidopsis*. *Proc. Natl. Acad. Sci. U.S.A.* **96**, 12941–12946 (1999).
8. E. B. Blancaflor, J. M. Fasano, S. Gilroy, Mapping the functional roles of cap cells in the response of *Arabidopsis* primary roots to gravity. *Plant Physiol.* **116**, 213–222 (1998).
9. H. Konnings, The significance of the root cap for geotropism. *Acta Bot. Sin.* **17**, 203–211 (1968).
10. S. Mancuso, P. W. Barlow, D. Volkmann, F. Baluska, Actin turnover-mediated gravity response in maize root apices: Gravitropism of decapped roots implicates gravisensing outside of the root cap. *Plant Signal. Behav.* **1**, 52–58 (2006).
11. C. Wolverton, J. L. Mullen, H. Ishikawa, M. L. Evans, Root gravitropism in response to a signal originating outside of the cap. *Planta* **215**, 153–157 (2002).
12. J. Z. Kiss, F. D. Sack, Severely reduced gravitropism in dark-grown hypocotyls of a starch-deficient mutant of *Nicotiana sylvestris*. *Plant Physiol.* **94**, 1867–1873 (1990).
13. F. Darwin, The statolith theory of geotropism. *Nature* **67**, 571–572 (1903).
14. N. Saether, T. H. Iversen, Gravitropism and starch statoliths in an *Arabidopsis* mutant. *Planta* **184**, 491–497 (1991).
15. J. Friml, J. Wiśniewska, E. Benková, K. Mendgen, K. Palme, Lateral relocation of auxin efflux regulator PIN3 mediates tropism in *Arabidopsis*. *Nature* **415**, 806–809 (2002).
16. G. B. Monshausen, H. E. Zieschang, A. Sievers, Differential proton secretion in the apical elongation zone caused by gravistimulation is induced by a signal from the root cap. *Plant Cell Environ.* **19**, 1408–1414 (1996).
17. J. M. Fasano *et al*., Changes in root cap pH are required for the gravity response of the *Arabidopsis* root. *Plant Cell* **13**, 907–921 (2001).
18. J. L. Mullen, H. Ishikawa, M. L. Evans, Analysis of changes in relative elemental growth rate patterns in the elongation zone of *Arabidopsis* roots upon gravistimulation. *Planta* **206**, 598–603 (1998).
19. G. Huang *et al*., Rice actin binding protein RMD controls crown root angle in response to external phosphate. *Nat. Commun.* **9**, 2346 (2018).
20. K. Boonsirichai, J. C. Sedbrook, R. Chen, S. Gilroy, P. H. Masson, ALTERED RESPONSE TO GRAVITY is a peripheral membrane protein that modulates gravity-induced cytoplasmic alkalinization and lateral auxin transport in plant statocytes. *Plant Cell* **15**, 2612–2625 (2003).
21. J. M. Guseman, K. Webb, C. Srinivasan, C. Dardick, DRO1 influences root system architecture in *Arabidopsis* and *Prunus* species. *Plant J.* **89**, 1093–1105 (2017).
22. I. K. Dawson *et al*., Barley: A translational model for adaptation to climate change. *New Phytol.* **206**, 913–931 (2015).
23. V. Talamè *et al*., TILLMore, a resource for the discovery of chemically induced mutants in barley. *Plant Biotechnol. J.* **6**, 477–485 (2008).
24. R. Bovina *et al*., Identification of root morphology mutants in barley. *Plant Genet. Resour.* **9**, 357–360 (2011).
25. S. Wu *et al*., VLN2 regulates plant architecture by affecting microfilament dynamics and polar auxin transport in rice. *Plant Cell* **27**, 2829–2845 (2015).
26. M. Mascher *et al*., A chromosome conformation capture ordered sequence of the barley genome. *Nature* **544**, 427–433 (2017).
27. C. Monat *et al*., TRITEX: Chromosome-scale sequence assembly of Triticeae genomes with open-source tools. *Genome Biol.* **20**, 284 (2019).
28. C. J. A. Sigrist *et al*., New and continuing developments at PROSITE. *Nucleic Acids Res.* **41**, D344–D347 (2013).
29. G. Denay, G. Vachon, R. Dumas, C. Zubieta, F. Parcy, Plant SAM-domain proteins start to reveal their roles. *Trends Plant Sci.* **22**, 718–725 (2017).
30. C. A. Hollender *et al*., Loss of a highly conserved sterile alpha motif domain gene (*WEEP*) results in pendulous branch growth in peach trees. *Proc. Natl. Acad. Sci. U.S.A.* **115**, E4690–E4699 (2018).
31. K. V. Krasileva *et al*., Uncovering hidden variation in polyploid wheat. *Proc. Natl. Acad. Sci. U.S.A.* **114**, E913–E921 (2017).
32. G. K. Kirschner, Y. Stahl, M. Von Korff, R. Simon, Unique and conserved features of the barley root meristem. *Front Plant Sci* **8**, 1240 (2017).
33. M. I. Love, W. Huber, S. Anders, Moderated estimation of fold change and dispersion for RNA-seq data with DESeq2. *Genome Biol.* **15**, 550 (2014).
34. D. J. Cosgrove, Plant expansins: Diversity and interactions with plant cell walls. *Curr. Opin. Plant Biol.* **25**, 162–172 (2015).
35. M. Taniguchi *et al*., The Arabidopsis LAZY1 family plays a key role in gravity signaling within statocytes and in branch angle control of roots and shoots. *Plant Cell* **29**, 1984–1999 (2017).
36. M. Hála *et al*., An exocyst complex functions in plant cell growth in *Arabidopsis* and tobacco. *Plant Cell* **20**, 1330–1345 (2008).
37. T. Ogura *et al*., Root system depth in *Arabidopsis* is shaped by EXOCYST70A3 via the dynamic modulation of auxin transport. *Cell* **178**, 400–412.e16 (2019).
38. N. Siddiqui, J. Léon, A. A. Naz, A. Ballvora, Genetics and genomics of root system variation in adaptation to drought-stress in cereal crops. *J. Exp. Bot.* **72**, 1007–1019. (2021).
39. Y. Kitomi *et al*., Root angle modifications by the *DRO1* homolog improve rice yields in saline paddy fields. *Proc. Natl. Acad. Sci. U.S.A.* **117**, 21242–21250 (2020).
40. G. Rubio *et al*., Root gravitropism and below-ground competition among neighbouring plants: A modelling approach. *Ann. Bot.* **88**, 929–940 (2001).
41. M. F. Dreccer *et al*., Genotypic variation for lodging tolerance in spring wheat: Wider and deeper root plates, a feature of low lodging, high yielding germplasm. *F. Crop. Res.* **258**, 107942 (2020).
42. W. Sinclair, I. Oliver, P. Maher, A. Trewavas, The role of calmodulin in the gravitropic response of the *Arabidopsis thaliana agr-3* mutant. *Planta* **199**, 343–351 (1996).
43. A. M. Jones *et al*., Border control–A membrane-linked interactome of *Arabidopsis*. *Science* **344**, 711–716 (2014).
44. F. Passardi, C. Penel, C. Dunand, Performing the paradoxical: How plant peroxidases modify the cell wall. *Trends Plant Sci.* **9**, 534–540 (2004).
45. J. H. Joo, Y. S. Bae, J. S. Lee, Role of auxin-induced reactive oxygen species in root gravitropism. *Plant Physiol.* **126**, 1055–1060 (2001).
46. A. Osthoff, P. Donà Dalle Rose, J. A. Baldauf, H. P. Piepho, F. Hochholdinger, Transcriptomic reprogramming of barley seminal roots by combined water deficit and salt stress. *BMC Genomics* **20**, 325 (2019).
47. D. C. Hoagland, D. I. Arnon, *The Water Culture Method for Growing Plant Without Soil* (College of Agriculture, University of California) (1950).
48. K. A. Nagel *et al*., GROWSCREEN-Rhizo is a novel phenotyping robot enabling simultaneous measurements of root and shoot growth for plants grown in soil-filled rhizotrons. *Funct. Plant Biol.* **39**, 891–904 (2012).
49. D. Pflugfelder *et al*., Non-invasive imaging of plant roots in different soils using magnetic resonance imaging (MRI). *Plant Methods* **13**, 102 (2017).
50. C. A. Schneider, W. S. Rasband, K. W. Eliceiri, NIH Image to ImageJ: 25 years of image analysis. *Nat. Methods* **9**, 671–675 (2012).
51. R. W. Michelmore, I. Paran, R. V. Kesseli, Identification of markers linked to disease-resistance genes by bulked segregant analysis: A rapid method to detect markers in specific genomic regions by using segregating populations. *Proc. Natl. Acad. Sci. U.S.A.* **88**, 9828–9832 (1991).
52. J. Comadran *et al*., Natural variation in a homolog of Antirrhinum CENTRORADIALIS contributed to spring growth habit and environmental adaptation in cultivated barley. *Nat. Genet.* **44**, 1388–1392 (2012).
53. D. L. Hyten *et al*., High-throughput genotyping with the GoldenGate assay in the complex genome of soybean. *Theor. Appl. Genet.* **116**, 945–952 (2008).
54. H. Li, R. Durbin, Fast and accurate short read alignment with Burrows-Wheeler transform. *Bioinformatics* **25**, 1754–1760 (2009).
55. H. Li *et al*.; 1000 Genome Project Data Processing Subgroup, The sequence alignment/map format and SAMtools. *Bioinformatics* **25**, 2078–2079 (2009).
56. H. Li, A statistical framework for SNP calling, mutation discovery, association mapping and population genetical parameter estimation from sequencing data. *Bioinformatics* **27**, 2987–2993 (2011).
57. P. Cingolani *et al*., A program for annotating and predicting the effects of single nucleotide polymorphisms, SnpEff: SNPs in the genome of *Drosophila* melanogaster strain w1118; iso-2; iso-3. *Fly (Austin)* **6**, 80–92 (2012).
58. D. van Dusschoten *et al*., Quantitative 3D analysis of plant roots growing in soil using magnetic resonance imaging. *Plant Physiol.* **170**, 1176–1188 (2016).
59. N. Kumar *et al*., Further analysis of barley MORC1 using a highly efficient RNA-guided Cas9 gene-editing system. *Plant Biotechnol. J.* **16**, 1892–1903 (2018).
60. G. R. Lazo, P. A. Stein, R. A. Ludwig, A DNA transformation-competent *Arabidopsis* genomic library in Agrobacterium. *Biotechnology (N. Y.)* **9**, 963–967 (1991).
61. J. Imani, L. Li, P. Schäfer, K.-H. Kogel, STARTS—A stable root transformation system for rapid functional analyses of proteins of the monocot model plant barley. *Plant J.* **67**, 726–735 (2011).
62. M. W. Pfaffl, A new mathematical model for relative quantification in real-time RT-PCR. *Nucleic Acids Res.* **29**, e45 (2001).
63. M. S. Anjam *et al*., An improved procedure for isolation of high-quality RNA from nematode-infected *Arabidopsis* roots through laser capture microdissection. *Plant Methods* **12**, 25 (2016).
64. A. Matei *et al*., How to make a tumour: Cell type specific dissection of Ustilago maydis-induced tumour development in maize leaves. *New Phytol.* **217**, 1681–1695 (2018).
65. A. M. Bolger, M. Lohse, B. Usadel, Trimmomatic: A flexible trimmer for Illumina sequence data. *Bioinformatics* **30**, 2114–2120 (2014).
66. A. Dobin *et al*., STAR: Ultrafast universal RNA-seq aligner. *Bioinformatics* **29**, 15–21 (2013).
67. S. Anders, P. T. Pyl, W. Huber, HTSeq—A Python framework to work with high-throughput sequencing data. *Bioinformatics* **31**, 166–169 (2015).
68. Y. Benjamini, Y. Hochberg, Controlling the false discovery rate: A practical and powerful approach to multiple testing. *R. Stat. Soc.* **57**, 289–300 (1995).
69. T. Tian *et al*., agriGO v2.0: A GO analysis toolkit for the agricultural community, 2017 update. *Nucleic Acids Res.* **45** (W1), W122–W129 (2017).
70. S. Kumar, G. Stecher, M. Li, C. Knyaz, K. Tamura, MEGA X: Molecular evolutionary genetics analysis across computing platforms. *Mol. Biol. Evol.* **35**, 1547–1549 (2018).
71. M. Nei, S. Kumar, *Molecular Evolution and Phylogenetics* (Oxford University Press, 2000).
72. D. T. Jones, W. R. Taylor, J. M. Thornton, The rapid generation of mutation data matrices from protein sequences. *Comput. Appl. Biosci.* **8**, 275–282 (1992).